TOPICAL REVIEW • OPEN ACCESS

The plateau in above-threshold ionization: the keystone of rescattering physics

To cite this article: W Becker *et al* 2018 *J. Phys. B: At. Mol. Opt. Phys.* **51** 162002

View the article online for updates and enhancements.

Topical Review

The plateau in above-threshold ionization: the keystone of rescattering physics

W Becker[1,2] **, S P Goreslavski**[2]**, D B Milošević**[1,3,4] **and G G Paulus**[5,6]

[1] Max-Born-Institut, Max-Born-Str. 2a, D-12489 Berlin, Germany
[2] National Research Nuclear University MEPhI, Kashirskoe Shosse 31, 115409, Moscow, Russia
[3] Faculty of Science, University of Sarajevo, Zmaja od Bosne 35, 71000 Sarajevo, Bosnia and Herzegovina
[4] Academy of Sciences and Arts of Bosnia and Herzegovina, Bistrik 7, 71000 Sarajevo, Bosnia and Herzegovina
[5] Institute of Optics and Quantum Electronics, Friedrich Schiller University, Max-Wien Platz 1, D-07743 Jena, Germany
[6] Helmholtz Institute Jena, Fröbelstieg 3, D-07743 Jena, Germany

E-mail: milo@bih.net.ba

Abstract

A review is presented of the rescattering plateau in laser-induced above-threshold ionization and its various features as they were discovered over time. Several theoretical explanations are discussed, from simple momentum conservation to the quantum-mechanical improved strong-field approximation and the inherent quantum orbits or, alternatively, entirely classical methods. Applications of the plateau to the extraction of atomic or molecular potentials and to the characterization of the driving laser pulse are also surveyed.

Keywords: plateau, above-threshold ionization, rescattering physics

(Some figures may appear in colour only in the online journal)

1. Introduction: looking back after 25 years

Much of the beauty of strong-field laser-atom physics originates in its three hallmark phenomena—non-sequential double ionization (NSDI) [1, 2] and the plateaus of high-order harmonic generation (HHG) [3–5] and above-threshold ionization (ATI) [6]—along with their coherent explanation in terms of classical or quantum orbits [7–10]. However, there has been more than mere beauty: concurrently, attosecond laser physics has developed by taking advantage of strong-field laser physics for the generation *and* the metrology of attosecond pulses and phenomena; for reviews, see [11–14].

From today's perspective, it appears that at the beginning of 1993 all pieces but one were in place allowing for a grand view of strong-field laser-atom physics: the plateau in HHG and its explanation by classical electron trajectories revisiting the parent ion [15, 16] and the famous NSDI 'knee' in the intensity dependence of the double ionization yield of rare gases [17], along with the absence of these effects for a circularly polarized laser field [18, 19]. The only missing piece, one might think today, would have been some 'plateau' in high-order ATI (HATI), analogous with the HHG plateau. In 1993, however, the perception was completely different as is evident from the report of an anonymous referee: 'It has been admitted for by now several years that ATI electron spectra do not exhibit the plateau behavior that characterizes HHG.' Moreover, the recollision picture was highly controversial. With respect to NSDI, the last sceptics were only convinced more than five years later by the first reaction-microscope experiments [20, 21]. Accordingly, when the ATI plateau was finally discovered at
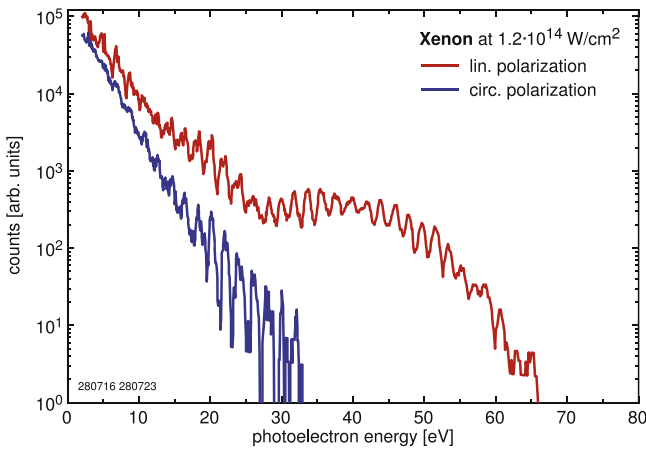
Figure 1. ATI spectra recorded in July 1993 using a femtosecond laser system consisting of a dye colliding-pulse mode-locked oscillator and a dye amplifier pumped by a copper-vapor laser. The wavelength was 630 nm, the pulse duration 40 fs, and the intensity corresponded to $U_p = 4.5$ eV. Besides the ATI plateau and its disappearance for circular polarization, also some of the effects referred to in the main text are visible, in particular varying ATI peak contrast and peak separations not equal to the photon energy.

the end of June 1993, rescattering was not at all everyone's first guess. This was in spite of the fact that slightly earlier 'rings' or 'side lobes' in the angle-dependent ATI spectrum had been detected [22] and submitted to a classical rescattering description almost as readily as the plateau itself [23].

In figure 1 we present a by now historical plot of a measured ATI spectrum, which illustrates why the geographical term 'plateau' was invoked to characterize the pronounced annex at high energies. Note that this annex would have completely escaped attention on a linear scale. The nomenclature 'plateau' was also drawing the analogy to HHG. The feature disappears for circular polarization, which provided the essential clue to its origin: rescattering.

Looking back today with the hindsight of almost 25 years at the data presented in [6], it is interesting to observe what was discussed at the time and what was not. Spectra were exhibited for all of the rare gases, and they were significantly different (krypton barely shows a change of slope rather than a plateau), but the universal validity of the rescattering picture was the dominant lesson drawn from the data, and the very obvious differences between the various rare gases were played down. By now, the perspective has been reversed: ATI and HATI are employed to extract atomic and molecular information from the data [24–32]. Another eye-catching feature of the spectra that received little attention is the existence of a group or groups of particularly well developed peaks in the middle of the plateau (above approx. 5 U_p, where U_p is the ponderomotive energy[7]), especially for argon, while the peaks at lower and at higher energies are less well developed and have much lower contrast. In this context, it

was remarked that '... the energy difference between a peak on the plateau and one at lower energies ... does not correspond to an integral number of photons' [6]. As we will see in section 3.1 this was a very important observation, which was not followed up on at the time.

We will, in this paper, consider the plateau and the further developments that it started. Today, it is clear that the plateau will gradually disappear when the laser polarization turns from linear to circular, but how fast will it go and how will its shape be affected? The first observation of the plateau was carried out for a fairly long pulse (40 fs). What is the effect of the pulse length on the plateau? Not yet in 1993, but some time later, pulses became so short that their specific shape started to play a role, for the direct electrons as well as, especially, the plateau. We will return to the early observation of the groups of exceptionally well developed peaks in the middle of the plateau and see that it provides the key to a much deeper understanding of the plateau and the underlying mechanism.

The guiding principle in our interpretation will be momentum conservation as it underlies the simple-man model [33]. It is embedded in the quantum-mechanical improved strong-field approximation (ISFA) from which it can be extracted via the saddle-point evaluation. The resulting theory has been called 'quantum-orbit theory' [7–10]. It will provide a unified framework for the interpretation. Its shortcoming is an incomplete consideration of the effects of the Coulomb potential. Almost all the effects mentioned thus far are related to *backscattering* of the revisiting electron. However, the returning electron can rescatter in any direction including the forward direction. This will lead to a new perspective of the so-called low-energy structure (LES) and other recently observed features of ATI for very low electron energy. As a very important application of ATI, we will discuss the determination of the carrier-envelope phase or absolute phase of a few-cycle laser pulse. Finally, we will completely change the description and reconsider ATI and the LES from an entirely classical point of view that includes the Coulomb potential exactly.

Before concluding this introduction, in figure 2 we schematically present the semiclassical three-step model, which embodies the generally accepted physical picture of the HATI process. When the field is close to an extremum, the electron, up to this time t_0 bound in the atom with the energy $-I_p$, can tunnel through the potential barrier and is 'born' in the continuum with zero velocity $v(t_0)$ (step 1). Thereafter, the electric field strength decreases and goes through zero to its next maximum positive value. Since the electric force at the time t' changes its sign when the field does, the electron turns around at the time t'' and starts returning to its parent ion. This is the second step of the three-step model. The corresponding electron velocity, as we will show in the next section, is related to the vector potential $\mathbf{A}(t)$, which is equal to zero at the times t_0 and t'' since $E(t) = -dA(t)/dt$ and the field is extremal at these times. By momentum conservation, the maximum electron kinetic energy at the return is $E_{\text{ret,max}} = v_{\text{drift}}^2/2 = 3.17\,U_p$ [15, 16]. In the third step, the electron elastically scatters off its parent ion and moves towards the detector. In the case of backscattering, the maximum electron energy at the detector is $E_{\text{bs,max}} = 10.007\,U_p$ [23] (for direct ionization, i.e. for ATI without

---

[7] An electron in a laser field cannot be at rest. At least, it has to wiggle following the acceleration due to the laser field, with no additional directional motion. The corresponding kinetic energy averaged over one cycle (of duration T) of the laser field is called the ponderomotive energy $U_p = \langle e^2 \mathbf{A}^2(t) \rangle_T/(2m)$.
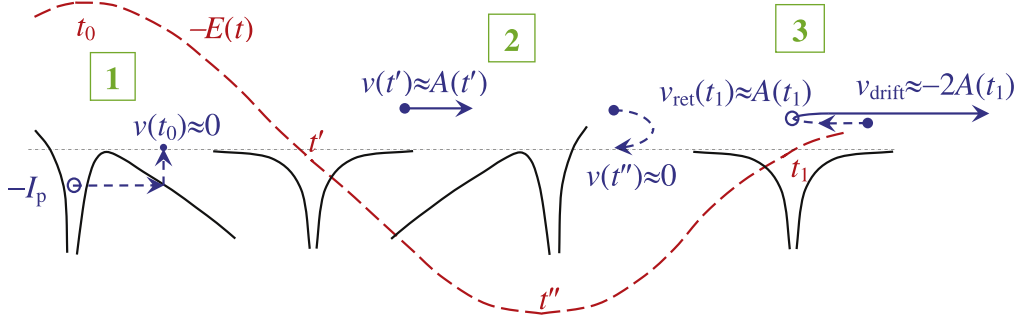
Figure 2. Graphical sketch of the three-step model as described in the text. The temporal evolution of a linearly polarized laser field $E(t)$ is represented by the red long-dashed line, the combined atom + laser field potential, $V(r) + \mathbf{r} \cdot \mathbf{E}(t)$, is depicted in black, while the electron and its velocity are in blue.

rescattering, we will show that $E_{\text{dir,max}} = 2\, U_{\text{p}}$). The probability of the HATI process is approximately the same for all final electron energies $2\, U_{\text{p}} < E_{\text{bs}} < 10.007\, U_{\text{p}}$ so that the corresponding photoelectron spectrum forms a plateau. This is a simple condensed explanation of the formation of the plateau. We will return to this in more detail later in the paper.

The topics to be considered have been covered by many more general review papers [34–41]. Some historical remarks can be found in [39]. The current paper will focus on the ATI plateau and its properties and applications as well as simple interpretations ranging from momentum conservation in the presence of only the laser field to the SFA and ISFA and quantum orbits.

2. The kinematics of recollision and momentum conservation

To a significant extent, the dynamics of strong-field ionization in general and rescattering in particular can be understood by the principle of momentum conservation. A fundamental approximation in strong-field laser physics is the assumption that ionization, i.e., the transition from the ground state to a continuum state, occurs at some well-defined instant t_0 (which is weighted and integrated over to obtain spectra and rates). Before ionization, for $t < t_0$, the laser field is assumed to have negligible effect on the electron, which is tightly bound. At $t = t_0$, horses are switched and the effect of the Coulomb field is neglected such that the equation of motion of the electron in the continuum is governed by the laser field alone. We will restrict ourselves to the nonrelativistic regime and employ the long-wavelength approximation for the laser field so that the electric field of the laser is assumed only to depend on time, $\mathbf{E}(\mathbf{r}, t) \to \mathbf{E}(t)$, and the magnetic field is ignored.

The equation of motion for $t > t_0$ therefore reads

$$m\dot{\mathbf{v}}(t) = -e\mathbf{E}(t), \tag{1}$$

where $\mathbf{v}$ is the electron's velocity and m and $-e$ denote its mass and charge. Whenever convenient, we will use atomic units, i.e. $m = e = 1$. Using $\mathbf{E}(t) = -\dot{\mathbf{A}}(t)$, we obtain

$$\frac{d}{dt}\left(m\mathbf{v}(t) - e\mathbf{A}(t)\right) = \mathbf{0}. \tag{2}$$

(If the field is described in length gauge, we use $\mathbf{A}(t)$ as shorthand for $-\int^t d\tau \mathbf{E}(\tau)$. In velocity gauge, $\mathbf{A}(t)$ is the vector potential and the generalized or canonical momentum is $\mathbf{p}_{\text{can}} := m\mathbf{v}(t) - e\mathbf{A}(t)$.) In any case, the quantity $m\mathbf{v}(t) - e\mathbf{A}(t)$ is conserved. Assuming tunneling at the time t_0, so that $\mathbf{v}(t_0) = \mathbf{0}$, we find $\mathbf{p}_{\text{can}} = -e\mathbf{A}(t_0)$. We normalize the vector potential by requiring that $\mathbf{A}(t \to -\infty) = \mathbf{0}$. Any laser pulse exerts a net force of zero on a free particle resulting in a net transferred momentum of zero, i.e., $\int_{-\infty}^{\infty} \mathbf{E}(t)\, dt = \mathbf{A}(-\infty) - \mathbf{A}(\infty) = \mathbf{0}$ [37], so that $\mathbf{A}(+\infty) = \mathbf{0}$ as well. Evaluating the conserved quantity $\mathbf{p}_{\text{can}}$ at infinity (after the end of the laser pulse), we realize the physical meaning of the canonical momentum as the electron's drift velocity, which is measured at a detector outside the field:

$$\mathbf{p}_{\text{can}} \equiv m\mathbf{v}_{\text{drift}} = -e\mathbf{A}(t_0). \tag{3}$$

This is often referred to as the simple-man model [33].

Before discussing recollisions, we demonstrate the predictive power of the conservation of the canonical momentum (as well as its limitations) at the example of photoelectrons that do not rescatter, the so-called direct electrons. A first, rather trivial example of an application of equation (3) is the prediction of the classical cutoff energy of direct electrons in quasi-monochromatic laser fields [33, 42]. It is evident that the maximum of $|\mathbf{A}(t)|$ equals its amplitude A_0. Recalling that (for linear polarization) the ponderomotive energy U_{p} is given by $U_{\text{p}} = e^2 A_0^2/(4m)$, we reproduce the well-known cutoff energy of $\mathbf{p}_{\text{can,max}}^2/(2m) = e^2 A_0^2/(2m) = 2\, U_{\text{p}}$. The drift velocity is largest when $|A(t_0)|$ reaches a maximum; but then $E(t_0) = -\dot{A}(t_0) = 0$, which means that no electrons are liberated at this time. In other words: the probability to detect photoelectrons decreases with increasing energy—a very familiar fact.

A less trivial example is the so-called attoclock [43–46], i.e., the photoelectron momentum distribution created by highly elliptically polarized laser fields. For a sufficiently long pulse, the parametric plots of $\mathbf{E}(t)$ (i.e. the polarization ellipse) and $\mathbf{A}(t)$ will be virtually identical. Therefore, considering equation (3), the instant of ionization within each optical cycle can be read off the azimuth of the photoelectron's momentum distribution. An example of such a measurement is displayed in figure 3 [47]. The remarkable feature
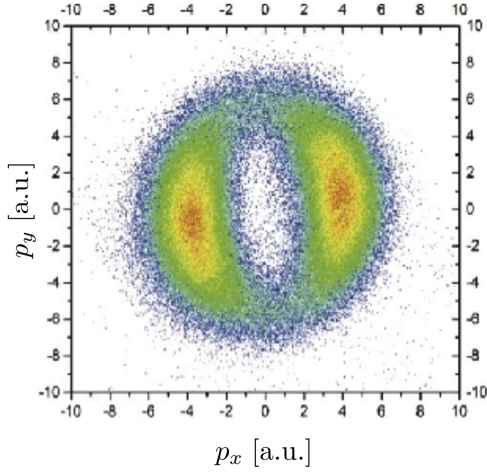
Figure 3. Ionization of Ne$^+$ ions in an ion-beam apparatus by elliptically polarized 30 fs laser pulses with an intensity of $\approx 10^{17}$ W cm^{-2} and ellipticity 0.74. The Ne^{2+}-ions are detected on a position- and time-resolving microchannel plate. The major polarization axis is parallel to the y direction. Nevertheless, most events are emitted to the x direction. However, the entire distribution appears to be skewed counterclockwise. Reprinted figure with permission from [47], copyright (2015) by the American Physical Society.

of these distributions is that most events are recorded in the direction of the *minor* axis, where the field strength is small. Although at first sight counterintuitive, it makes perfect sense considering equation (3): the phase of $\mathbf{A}(t)$ is shifted by 90° with respect to the phase of $\mathbf{E}(t)$, at least for a monochromatic wave; see [48] where the effect was called 'dodging'—the electron appears to dodge the strong force. However, it must not be overlooked that the yield does *not* maximize exactly in the direction of the minor polarization axis. This observation gave rise to a still unsettled discussion about a finite tunneling time [49, 50], but it should not be forgotten that a number of approximations were made: (i) the Coulomb force has been neglected; in its presence momentum conservation no longer holds [51, 52]. (ii) The time-dependence of the amplitude has been neglected. The shorter the pulse duration is, the less accurate will be the statement that $\mathbf{E}(t)$ and $\mathbf{A}(t)$ are perpendicular. (iii) Ground state depletion has been neglected. But most experiments are performed close to saturation of ionization. Therefore, if depletion of the ground state plays a role, the ionization yield decreases from cycle to cycle and is in the first half of each cycle slightly larger than in the second. For a discussion of the contributions of these and other effects to the tunneling time, see [53].

Momentum conservation can also be applied to explain the kinematics of recollision. In fact, some of the approximations just mentioned are not very relevant for the corresponding effects, i.e. the conclusions obtained can be expected to be quite robust. Recollision implies that the electron returns to the ion core at some time $t_1 > t_0$, is scattered, and subsequently further accelerated by the laser field. The simplest but arguably most prominent case is that the recolliding electron is scattered backward. This means (we consider, for now, linear polarization so that all vectors only have one component; we

also introduce the infinitesimally small positive time ε)

$$mv(t = t_1 - \varepsilon) = -mv(t = t_1 + \varepsilon). \tag{4}$$

The momentum immediately before rescattering is the opposite of the momentum immediately thereafter. Next, momentum conservation is applied twice: $p_{\text{can}}(t_0) = p_{\text{can}}(t_1 - \varepsilon)$, i.e.

$$mv(t = t_1 - \varepsilon) = eA(t_1) - eA(t_0), \tag{5}$$

and $p_{\text{can}}(t_1 + \varepsilon) = p_{\text{can}}(t \to \infty)$, i.e.

$$mv(t = t_1 + \varepsilon) - eA(t_1) = p_{\text{drift}}. \tag{6}$$

Substitution of equations (4) and (5) in equation (6) then results in the drift momentum of the backscattered photoelectron:

$$p_{\text{drift}} = -2eA(t_1) + eA(t_0). \tag{7}$$

In order to make use of equation (7), the functional dependence of t_1 on t_0 must be known. It can be derived starting again with momentum conservation analogous to equation (5), $mv(t) = eA(t) - eA(t_0)$. Integration yields the position, $x(t) = F(t) - F(t_0) - (t - t_0)\dot{F}(t_0) + x(t_0)$, where $F(t) = \int^t A(t')dt'$. The condition of recollision, $x(t_1) = x(t_0)$, becomes

$$F(t_1) = F(t_0) + (t_1 - t_0)\dot{F}(t_0), \tag{8}$$

which has an obvious and instructive graphical interpretation [54], see figure 4. The ionization and recollision times, t_0 and t_1, that result in the trajectory with the largest drift velocity p_{drift} after rescattering are easily found by maximizing p_{drift} of equation (7) with respect to t_0 subject to the return condition (8). This yields the trigonometric equation $(1 - \tau \cot \tau)(1 - 2\tau \cot \tau) = 2\tau^2$ for $\tau = \omega(t_1 - t_0)/2$ as well as $\cot \sigma = \cot \tau - 1/\tau$ for $\sigma = \omega(t_1 + t_0)/2$. Numerically, for a cosine-shaped electric field waveform, the result is $\omega t_0 = 14.9°$ and $\omega t_1 = 261.6°$ for the first return. Using equation (7), one reproduces the well-known ATI plateau cutoff energy of 10.007 U_{p} [23].

The cutoff energy marks the end of the rescattering plateau. Figure 5 allows one to read off the travel time that corresponds to this and to other cutoff energies. The figure also shows that for any energy E smaller than the 10.007 U_{p} cutoff there are two different travel times, each corresponding to a certain start time t_0 and recollision time t_1, that yield this energy. These electrons form the plateau. Its height is primarily determined by the magnitude of the electric field at the start time t_0. Generally, both in this model and in reality, the height of the plateau varies rather smoothly with energy. An important feature that also determines its height is the magnitude of the rescattering matrix element, which occurs in the quantum description [26–29]. Finally, quantum mechanics will carve a very rugged structure into the plateau owing to interference of the contributions of the various start times. However, due to focal averaging this is rarely seen in experiments.

Figure 4 illustrates the possibility that the liberated electron may return to its parent ion more than twice. Consider, for example, the green straight line in figure 4, which is tangent to $F(t)$ at $t = t_0$. It intersects the curve $F(t)$ at $t = t_1$, $t = t_2$, and $t = t_3$. Hence, the crucial scattering event may also take place at the second, the third or even at later revisits.
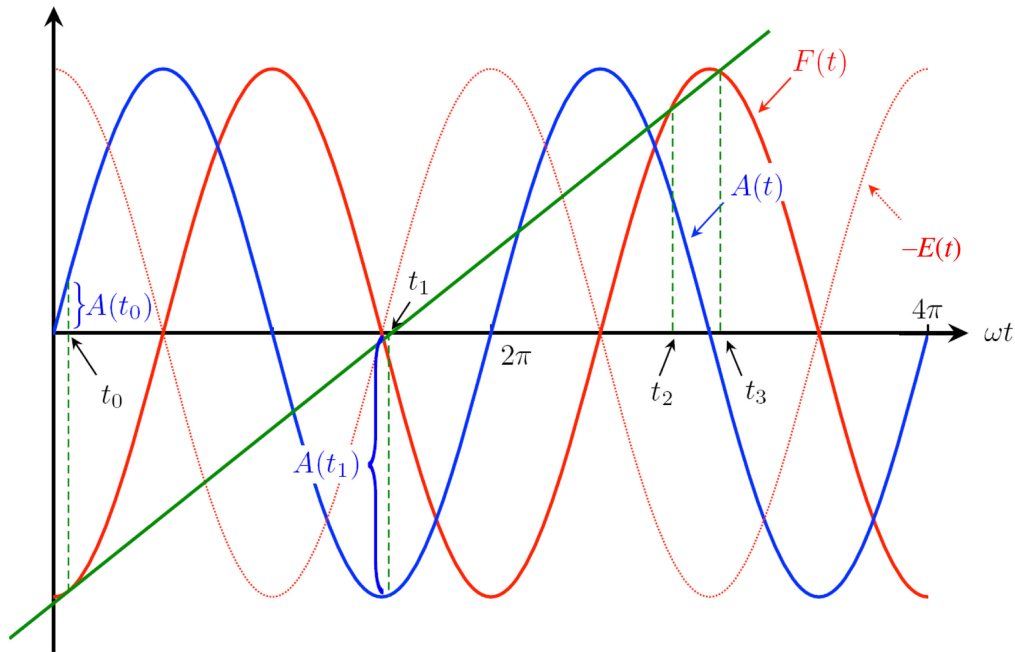
Figure 4. Graphical method for determining the recollision time t_1 for an electron liberated at t_0: a tangent (green) is aligned with $F(t)$ at $t = t_0$. The instant where it intersects $F(t)$ again defines the (first) recollision time t_1. Depending on the value of t_0, more than one recollision may occur. In the example given, there are two additional intersections at $t = t_2$ and $t = t_3$. If t_0 is slightly increased to $\tilde{t}_0$, the times $\tilde{t}_2$ and $\tilde{t}_3$ merge, i.e., the new tangent is a tangent also at $t = \tilde{t}_2 = \tilde{t}_3$. This means that the electron returns with zero velocity, in a 'soft recollision'. This kinematical situation generates the LES. For start times later than this $\tilde{t}_0$, there is only one recollision. Multiple recollisions (which give rise to 'long orbits') are responsible for intensity-dependent enhancements of groups of peaks in the rescattering plateau. Notice, that in the example the value of t_0 is just after a maximum of $-E(t)$ so that ωt_1 is very close to (but not identical with) $3\pi/2$. All the interesting rescattering physics that is due to multiple returns is generated by orbits that start very shortly after an extremum of $F(t)$. It should be noted that $F(t)$ is proportional to $E(t)$ for sufficiently long quasi-monochromatic laser pulses. However, equation (8) holds and the method can be used for arbitrary laser fields.
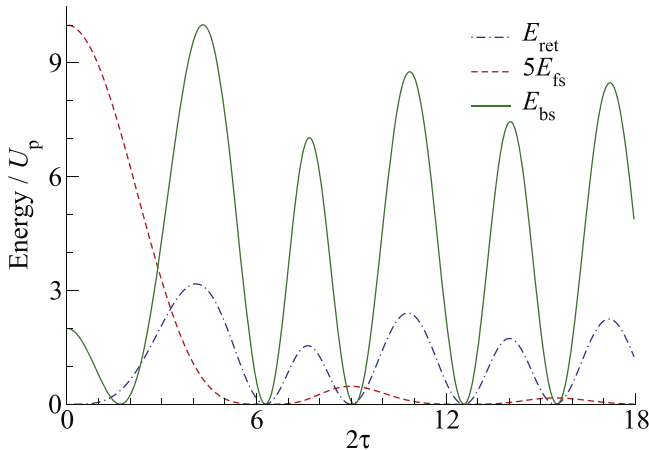

Figure 5. The return energy E_{ret} (dotted–dashed (blue) line), five times the forward scattering energy E_{fs} (dashed (red) line) and the backscattering energy E_{bs} (solid (green) line) as functions of the travel time $2\tau = \omega(t_1 - t_0)$. Conversely, for any fixed energy $E < 10.007\,U_p$ the intersections of a horizontal line with the curve E_{bs} afford the travel times such that the backscattered electron will arrive at the detector with the energy E. This makes clear that the contributions to any given energy E come in pairs, with the two members of a pair merging at the respective cutoff energy. Adapted from [55]. © IOP Publishing Ltd. All rights reserved.

The same information is presented differently in figure 5, where the final energy after backscattering is plotted versus the 'travel time,' that is, the difference between the rescattering time and the ionization time. (The figure also displays the final energy after *forward scattering*, to be discussed below and, for comparison, the energy at the time of return, which is the relevant quantity for HHG.) As functions of the travel time, the curves display maxima, which lead to sharply defined cutoffs in the spectra. In quantum mechanics, these cutoffs will be smoothed but still be very visible. Typically, just before such a cutoff the yield rears up and, subsequently, drops quickly after the cutoff.

For the second and third return, backscattering cutoff energies of approximately $7\,U_p$ and $8.7\,U_p$ can be read off from figure 5. For later and later returns, the cutoffs converge to $8\,U_p$ (see also figure 8 in [34]). The reason can be easily seen in figure 4: in order to afford later and later returns, the slope of the tangent must become smaller and smaller which implies that $F(t_0)$ will become extremal and thus $A(t_0) \to 0$. The drift momentum (7) after rescattering can then only be maximized by demanding $F(t_n) = 0$ and $A(t_n) \to A_0$. So we will have $p_{drift} \to 2A_0$, which indeed corresponds to the energy $8\,U_p$.

2.1. The LES

The discovery of the LES [56, 57] came as a surprise, because the low-energy region was considered fully understood at the time. The effect is in fact particularly pronounced at long wavelengths, i.e. for parameters for which the established models were believed to be particularly reliable. The experiments exhibiting the LES were made possible by various
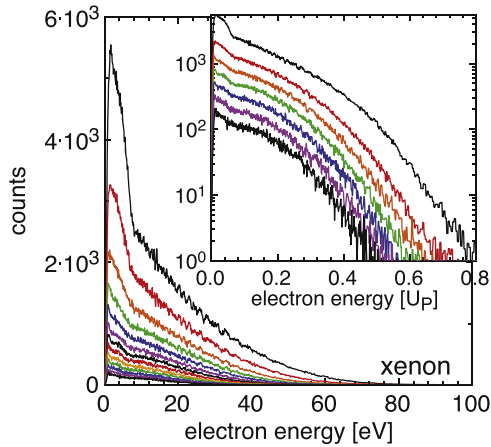
Figure 6. Photoelectron spectra of xenon in dependence of the intensity of 3.6 μm, 140 fs laser pulses. The laser intensity used to generate the spectra shown in the main panel was varied in steps of $0.025 \cdot I_0$, where $I_0 = 0.65 \times 10^{14}$ W cm^{-2} is the maximum laser intensity. The spectra of both gases exhibit a spike-like enhancement for $E \lesssim 10$ eV. The inset displays the xenon spectrum on a semi-logarithmic scale.

novel laser systems developed over many years [58]. Figure 6 exhibits an example showing unpublished spectra obtained during the initial phase of work that eventually resulted in [56]. The data are presented both on a linear scale and a logarithmic scale. On the linear scale it becomes clear that the LES is not a small effect at all. The log-scale data, especially at the highest intensity, already suggest that this feature is another plateau at low-energy; see below. On both scales, the LES appears on top of a distribution as it would be expected from pure tunneling.

It was immediately proposed that the LES might be related to forward rescattering [59]. Indeed, figure 5 exhibits forward scattering cutoffs at very low-energy. Figure 4 makes clear that the cutoff corresponds to a return with zero velocity. For such a soft recollision we have $\dot{F}(t_n) = \dot{F}(t_0) = 0$ at the return time. Figure 4 also shows that such a soft recollision is invariably preceded by one (or several) 'hard' recollisions where the electrons returns with substantial velocity. For an infinitely long monochromatic laser field, say $A(t) = A_0 \sin \omega t_0$ as it underlies figure 4, symmetry implies that this occurs at $\omega t_1 = (2n + 1)\pi/2$ with $n = 1, 2, ...$ where $F(t_1) = 0$. The corresponding start time t_0 is determined by equation (8), which yields $((2n + 1)\pi/2 - \omega t_0)\tan \omega t_0 = 1$. For $\omega t_0 \ll 1$, this can be trivially solved to retrieve the well-known LES energies [60, 55, 61, 62]

$$E_{\mathrm{LES}n} = \frac{8 \, U_{\mathrm{p}}}{(2n + 1)^2 \pi^2} \quad (n = 1, 2, ...). \quad (9)$$

The red dashed line in figure 5 makes clear that these are the cutoff energies for forward scattering. As such, they should give rise to pronounced cutoff features in the spectrum. The LES energies (9) can be considered as cutoffs of low-energy plateaus, in complete analogy with the high-energy plateau and its cutoff. Of course, the lengths of the low-energy plateaus are very short and only identifiable for midinfrared lasers. It is

interesting that low-energy plateaus, with the same cutoff energy positions as for forward scattering, also exist for backscattered electrons [63, 64].

The LES energies are very small and lie in an energy region that should be dominated by the direct electrons. This was the reason that until recently no one paid attention to rescattering, especially forward scattering, into states with low-energy. However, the liberated electron is subject to the Coulomb potential, and its forward scattering cross section is very large. This is why on the background of direct electrons forward-rescattered electrons may actually not only be visible but even be dominant [65]. This argument implies that LESs should not be visible for photodetachment of negative ions where the electron–ion potential is of short range and the scattering cross section is small.

The LES has attracted a lot of interest and was examined from various different angles and view points [61, 62, 66–70]. Following its discovery various additional spectral features at comparatively low energies have been identified: a very low-energy structure (VLES) significantly below the LES [71], a zero-energy structure (ZES) [72, 73], a 'V' structure [74–76], as well as other patterns in the velocity map at low-energy. All but the VLES can be attributed to low-energy rescattering, but other mechanisms have been discussed as well. Already before the discovery of the LES, a double-hump structure in the longitudinal momentum was observed [77, 78]. We will not further dwell on these effects whose origin is not yet entirely clear.

2.2. Rescattering in an arbitrary direction: laser-induced elastic diffraction

Equation (7) can also be regarded as a vector equation and thus describe not only the special cases of elastic backward or forward scattering. Rather, the electron recolliding with momentum $\mathbf{p}(t_1 - \varepsilon)$ may scatter in any direction. Figure 7 presents the angular-dependent cutoffs of a large number of orbits, which can be calculated analytically [79–81]. We anticipate that classical cutoffs tend to produce the most visible features in quantum-mechanical quantum-orbit calculations, which are in qualitative agreement with more exact simulations such as solutions of the time-dependent Schrödinger equation (TDSE) [82, 83]. Hence, the classical cutoffs can be expected to manifest themselves in experimental data. The figure exhibits an especially dense concentration of cutoffs around the origin, including for zero transverse momentum the series (9) of LESs. Some of the other afore-mentioned patterns are visible here, such as the 'fork' and the 'V' structure [74–76], which have indeed been observed in experiments.

The region of the velocity map for comparatively large longitudinal momenta p_x and nonzero transverse momenta p_y can be exploited to extract the electron–ion scattering cross section from HATI data as the latter determine the angular distribution of ionization events along the rescattering circles [27–30, 84, 85]. For elastic scattering, the momenta of the scattered electrons will form a circle of radius $p(t_1) = e|A(t_1) - A(t_0)|$, see equation (5). Invoking conservation of momentum just as in the special case of backscattering, it is
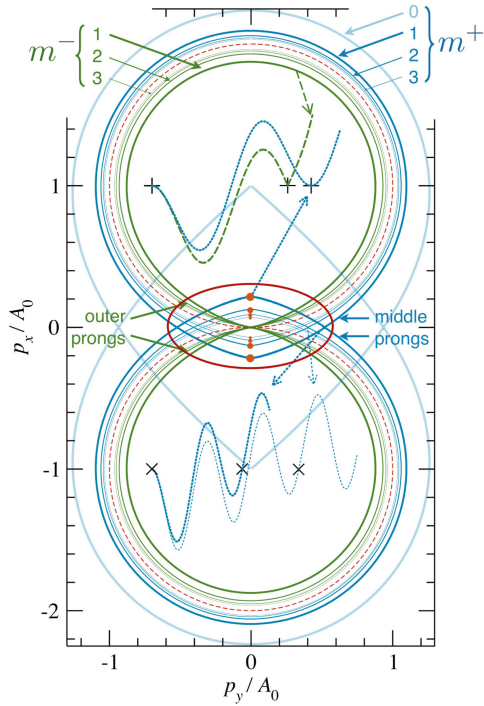
J. Phys. B: At. Mol. Opt. Phys. **51** (2018) 162002

Topical Review

Figure 7. Angle-dependent cutoffs of the electron drift energy $E_{\mathrm{kin}}(\theta) = p^2(\theta)/2$; see [79–81]. On the p_x axis, we see the cutoffs corresponding to 10.01 U_{p} and then to 8.77 U_{p}, 8.48 U_{p} etc (blue curves, labeled $m^+ = 0$, 1, 2, ...) above 8 U_{p}, and to 7.03 U_{p}, 7.45 U_{p} etc (green curves, labeled $m^- = 1$, 2, ...) below 8 U_{p}. The two sets converge to two 'limit circles', one for $p_x > 0$ and the other for $p_x < 0$, which intersect the vertical axis at $p_x = \pm\sqrt{2 \cdot 8\,U_{\mathrm{p}}} = 2A_0$ and are represented by the dashed (red) curves. They are exact circles and are tangential to the horizontal axis at the origin. Near the origin, for $p_y = 0$, we see the LES energies at 0.094 U_{p}, 0.033 U_{p}, ... marked by solid circles (orange). The two insets show several longitudinal (x component) simple-man orbits. The orange ellipse at the center of the figure identifies the region relevant for the 'fork' and the 'V' structure. Reprinted figure with permission from [55], copyright (2014) by the American Physical Society.

obvious that the scattering circles will be offset from the origin by the vector $e\mathbf{A}(t_1)$. The situation is depicted in figure 8 for the recollision time (or rather phase) of 261.6°, which has already been discussed for backscattering.

Figures 4 and 5 make clear that the electron has more than one option to get from the initial bound state into a given final state (with drift momentum $\mathbf{p}$). Namely, it may go there directly, or after having revisited its parent ion once or several times. The question arises how to add the contributions of these different scenarios. The answer requires quantum mechanics, which specifies the phases of the various contributions, which have to be superimposed coherently. The result of adding many such paths may be anywhere between constructive interference, which will strongly enhance the ionization rate, or a more or less random superposition, which will suppress it, or even complete destructive interference.

The backbone of a quantum-mechanical description of strong-field ionization that allows for rescattering is the ISFA. Next, we will briefly reproduce the most important results.

3. Quantum-mechanical SFA

The solution of the TDSE can be decomposed into two wave packets (we use atomic units from here on so that $\hbar = 1$, $m = 1$, and $e = 1$)

$$|\psi(t)\rangle - |\psi_0(t)\rangle = -i \int_{t_0}^{t} d\tau\, U_V(t, \tau) H_I(\tau) |\psi_0(\tau)\rangle$$
$$+ (-i)^2 \int_{t_0}^{t} d\tau \int_{t_0}^{\tau} d\tau'\, U_V(t, \tau) V U(\tau, \tau') H_I(\tau') |\psi_0(\tau')\rangle \quad (10)$$

(see, e.g., [34]) of which the first incorporates no interaction of the freed electron with the binding potential $V(\mathbf{r})$, while the second includes at least one. In equation (10), the state $|\psi_0(t)\rangle$ denotes the initial bound state, $H_I(t) = \mathbf{r} \cdot \mathbf{E}(t)$ is the electron-field interaction, and $U(t, t')$ and $U_V(t, t')$ represent the exact and the Volkov time-evolution operators, respectively. The latter can be expanded

$$U_V(t, \tau) = \int d^3\mathbf{k}\, |\psi_{\mathbf{k}}^V(t)\rangle \langle \psi_{\mathbf{k}}^V(\tau)|, \quad (11)$$

in terms of the Volkov states

$$|\psi_{\mathbf{k}}^V(t)\rangle = |\mathbf{k} + \mathbf{A}(t)\rangle \exp\left(-\frac{i}{2} \int_{t_0}^{t} d\tau\, (\mathbf{k} + \mathbf{A}(\tau))^2\right). \quad (12)$$

This way, we end up with an expansion of the final state

$$|\psi(t)\rangle - |\psi_0(t)\rangle = \int d^3\mathbf{p}\, |\psi_{\mathbf{p}}^V(t)\rangle (M_{\mathbf{p}}^{(0)}(t) + M_{\mathbf{p}}^{(1)}(t)), \quad (13)$$

which allows us to read off the amplitudes for direct ionization (direct electrons, SFA) [86–89]

$$M_{\mathbf{p}}^{(0)}(t) = -i \int_{t_0}^{t} d\tau\, \langle \psi_{\mathbf{p}}^V(\tau) | H_I(\tau) | \psi_0(\tau)\rangle \quad (14)$$

and for ionization with at least one act of rescattering [8, 90–98]

$$M_{\mathbf{p}}^{(1)}(t)$$
$$= (-i)^2 \int_{t_0}^{t} d\tau \int_{t_0}^{\tau} d\tau'\, \langle \psi_{\mathbf{p}}^V(\tau) | V U(\tau, \tau') H_I(\tau') | \psi_0(\tau')\rangle. \quad (15)$$

The fact that the direct term (14) is the lowest-order term of a Born series was already mentioned in [89]. To make the rescattering amplitude amenable to evaluation one usually replaces the exact propagator $U(t, \tau)$ by the Volkov propagator $U_V(t, \tau)$ (equation (11)). The result incorporates precisely one act of rescattering and is sometimes referred to as the ISFA. The amplitudes (14) and (15) are evaluated in the limit of $t \to \infty$.

Most of the theoretical results to be presented will be based on the amplitudes (14) and (15). The integrals over the ionization time τ in equation (14) and the ionization time τ' and the rescattering time τ in equation (15) can be carried out entirely numerically. However, the approximate evaluation with the help of the saddle-point method is much quicker and, moreover, affords a great deal of physical insight. We illustrate it in the case of the rescattering amplitude (15) (with $U \to U_V$). Inserting the expansion (11) for the Volkov propagator we collect all the exponentials that contribute to the
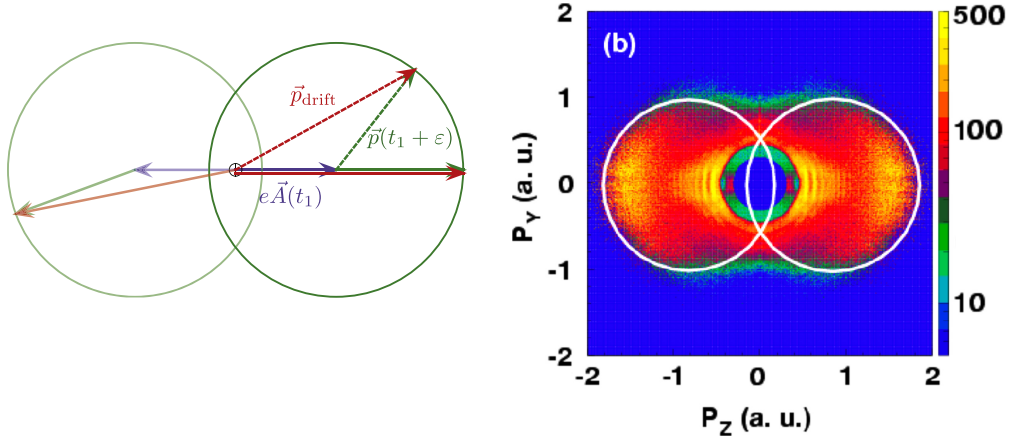
Figure 8. Momentum conservation and scattering circles in ATI: the momenta of elastically scattered electrons recolliding with momentum $\mathbf{p}(t_1)$ will form a corresponding scattering circle. Since the laser field is nonzero after the scattering event, the electrons are further accelerated, a process that can easily be described by conservation of canonical momentum. The left-hand panel displays the situation for $\omega t_1 = 261.6°$, which corresponds to the ATI cutoff trajectory. The kinetic energy of these electrons at the instant of recollision is $3.11 \, U_p$ and thus $|\mathbf{p}(t_1)| = \sqrt{3.11/2} \, eA_0 = 1.247 A_0$. The respective circle is displaced by $A_0 \sin(261.6°) = -0.99 A_0$. In case of backscattering, the total momentum is $-2.237 A_0$ which corresponds to an energy of $10 \, U_p$. For the subsequent half-cycle the same will take place in the opposite direction. The mechanism is beautifully confirmed experimentally, as shown in the right-hand panel. Reprinted figure with permission from [28], copyright (2008) by the American Physical Society.

integrand. Requiring that the resulting exponential be stationary with respect to its variables τ, τ', and $\mathbf{k}$ determines the saddle points:

$$(\mathbf{k} + \mathbf{A}(\tau'))^2 = -2I_p, \tag{16a}$$

$$\mathbf{k}(\tau - \tau') = -\int_{\tau'}^{\tau} d\sigma \mathbf{A}(\sigma), \tag{16b}$$

$$(\mathbf{k} + \mathbf{A}(\tau))^2 = (\mathbf{p} + \mathbf{A}(\tau))^2. \tag{16c}$$

The first equation describes energy conservation when the electron tunnels from its initial state with ionization potential I_p to a Volkov state with velocity $\mathbf{k} + \mathbf{A}(\tau')$. The second equation enforces that this electron, which started its trajectory at the time τ' at the center of the binding potential $V(\mathbf{r})$, return to this position at the time τ. Finally, the third equation describes elastic scattering at the time τ (above, in equation (4), we considered the special case of backscattering). Equations (16) are illustrated in figure 2. Obviously, equation (16a) does not allow for real solutions for τ' and, in consequence, all saddle points $(\tau, \tau', \mathbf{k})$ are complex. The solutions of the saddle-point equations define complex trajectories $\mathbf{x}(t)$ in space as a function of time t, which are called quantum orbits. Their real parts $\text{Re} \, \mathbf{x}(t)$ are closely related to the trajectories of the simple-man model, but owing to the imaginary parts, the trajectories do not start at the position of the ion but rather at the exit of the tunnel; see the orbits depicted in figure 10. For $I_p = 0$, the solutions are real (for linear polarization and provided the final energy is not too high). Equation (16a) then implies that the electron start its orbit with velocity $\mathbf{k} + \mathbf{A}(\tau') = \mathbf{0}$, which determines the tunnel exit time of the simple-man model. More details can be found in [9, 34, 37].

In figure 5, the energies for backscattering and forward scattering are plotted as a function of the time between return and ionization [60, 79]. This figure makes it easy to find these

times for given drift energy while the preceding figure 4 tells at which times an electron that started at a given ionization time $t_0 = \tau'$ will return. Especially, it becomes clear that for energies smaller than $8 \, U_p$ there are infinitely many solutions of the saddle-point equations (16). We denote them by $(\tau, \tau', \mathbf{k})|_s$ ($s = 1, 2, ...$). Only a subset $\tilde{s}$ must be used to construct the ionization amplitude. (This is related to the deformation of the original contour of integration, which is the real $(\tau, \tau', \mathbf{k})$ hyperplane, into the pertinent complex hyperplane. Only a subset of the saddle-point solutions will come to lie on the deformed contour.) This yields the saddle-point approximation

$$M_{\mathbf{p}}^{(0)} = \sum_{\tilde{s}} M_{\mathbf{p}}^{(0)}|_{\tilde{s}}, \qquad M_{\mathbf{p}}^{(1)} = \sum_{\tilde{s}} M_{\mathbf{p}}^{(1)}|_{\tilde{s}}. \tag{17}$$

For the direct amplitude $M_{\mathbf{p}}^{(0)}$, the set $\tilde{s}$ consists of only two solutions per cycle (for a monochromatic field). For the rescattering amplitude and large electron energies, figure 5 shows that the solutions $\tilde{s}$ also come in pairs. The orbits of the pair that corresponds to the cutoff energies are commonly called the long and the short orbit (this name was originally introduced for HHG, which also can be treated using the saddle-point method [7]). Coherent superposition of the direct orbits yields a characteristic pattern in the velocity map, which has been called the 'carpet' [99–101]. The interference of direct and rescattered amplitudes yields features that are related to the holographic structures [102, 103]. The decomposition of the ionization amplitude in terms of quantum orbits is closely analogous to Feynman's path integral [82, 104–106].

The main problem of the ISFA is the fact that the potential is only accounted for in first-order Born approximation. While for pure Coulomb scattering the latter happens to yield the exact scattering cross section, this is, of course, not so in the presence of an external laser field. Many

different attempts have been made to include the Coulomb field into the phases of the quantum orbits or, starting from a completely classical description, to augment the classical orbits by suitable phases [66, 67, 107–116]. The exact relation of these approaches to the ISFA is not known. In many instances, they improve the agreement with numerical solutions of the TDSE and experimental data. However, they do not include large-angle scattering and its associated effects.

Originally, owing to the absence of the long-range Coulomb force acting on the detached electron the SFA was proposed to apply for photodetachment of negative ions [86–89]; see also [117]. The same restriction should even more so apply for the ISFA. Not with standing, both have been employed mostly for atoms where they work surprisingly well though the presence of the Coulomb potential does cause substantial discrepancies. However, for negative ions the (I)SFA should provide an excellent description. Indeed, photodetachment experiments of F^- [118] were generally very well reproduced by the ISFA [119] and also by the time-dependent effective-range theory [120]. The F^- experiments also recorded 'energetic' electrons whose origin, whether by rescattering or by the slower dropoff of the direct-electron spectrum for the p ground state of F^-, remained unresolved. The confirmation that negative ions do exhibit a rescattering plateau in perfect agreement with the ISFA was accomplished for Br^- [121].

3.1. Intensity-dependent enhancements in the ATI plateau

For the rescattering amplitude $M_{\mathbf{p}}^{(1)}$, figure 5 shows that there are several solutions to the saddle-point equations (16) that must be included in the sum (17), at least two for $E_{\mathbf{p}}$ just below $10\,U_{\mathrm{p}}$ and infinitely many for $E_{\mathbf{p}} < 8\,U_{\mathrm{p}}$. The corresponding quantum orbits have been called the 'longer orbits'. Closer inspection has shown that for intensities such that

$$I_{\mathrm{p}} + U_{\mathrm{p}} = n\omega \tag{18}$$

with integer n, the coherent superposition of many long orbits is constructive for certain groups of HATI peaks in the plateau; for a formal analytical proof, see [81, 122]. The condition (18) means that the ponderomotively upshifted continuum threshold is multiphoton resonant with the ground state. This provides an explanation of one of the most conspicuous features of the ATI plateau, viz. the appearance of groups of peaks with enhanced yield and increased contrast in the spectrum [123–129]. Namely, in general, the ATI peaks are located at the energies

$$E_{\mathbf{p}} \equiv \mathbf{p}^2/2 = k\omega - U_{\mathrm{p}} - I_{\mathrm{p}}, \tag{19}$$

with integer k. Equations (18) and (19) imply that the peaks of an enhanced group occur at

$$E_{\mathbf{p}} = \ell\omega \tag{20}$$

with integer ℓ. In the focus of a laser pulse, there is invariably a distribution of intensities. The channel closing condition (18) is not necessarily satisfied by the peak intensity but by one (or several) lower intensities. Regardless, enhanced peaks
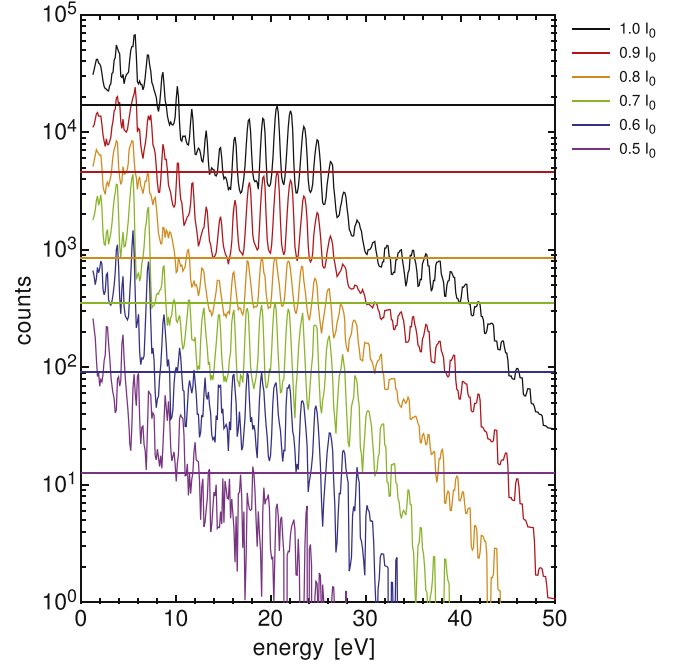

Figure 9. ATI spectra in argon at 800 nm in the direction of the linearly polarized laser field for the intensities 0.5, 0.6, 0.7, …, 1.0 I_0 with $I_0 = 0.8 \times 10^{14}\,\mathrm{W\,cm^{-2}}$. The horizontal lines mark the maxima of the plateaus for each intensity. Between the intensities $0.8I_0$ and $0.9I_0$ where the 12-photon channel closing moves into resonance, the yield jumps up and the contrast increases. Reprinted figure with permission from [129], copyright (2001) by the American Physical Society.

will be found at the energies (20). However, lower-order ATI peaks will be centered at energies (19) corresponding to the peak intensity. Hence, the energy difference between two peaks, one from a group of enhanced peaks (satisfying equation (20)) and the other one at much lower energy (satisfying equation (19) with the peak intensity), will not necessarily correspond to an integer multiple of ω. This was already noticed in the first report of the plateau [6]. These intensity-dependent resonances are one of the most intriguing effects in ATI. An example is presented in figure 9. The mechanism just advertised is only one of several explanations that have been proposed. Others are based on multiphoton resonance with intensity-dependent excited states [130–133] or subsume the effect [134–136] under the general mechanism of threshold anomalies [137, 138]. The fact that so many apparently different mechanisms have been successfully invoked is one of the fascinating aspects of the effect. We notice finally that multiphoton resonance with intensity-dependent upshifted states is not conceptually very different from the mechanism that we have advanced. Namely, the ISFA does not account for any excited bound states, so the only analogous feature is the continuum threshold, which is, of course, ponderomotively upshifted. In this sense, the ISFA is a zero-range-potential theory in disguise, because this potential does not support any excited bound states at all [129].

It was shown that the intensity-dependent enhancements fade away in the case where the driving pulse approaches a

J. Phys. B: At. Mol. Opt. Phys. **51** (2018) 162002

Topical Review

few-cycle pulse [139]. If the enhancements are due to constructive interference of the contributions of long quantum orbits, this is completely evident, since long orbits cannot unfold for short pulses. In the opposite case, for very long pulses, ISFA simulations show that the spectral shape of the enhancements develops extremely sharp, even divergent, spikes [81, 140].

3.2. Elliptical polarization

Momentum conservation remains the governing principle even when the laser field is elliptically polarized. We exploited this already for the direct electrons in the analysis of the attoclock. However, for rescattering, to make sure that the electron return to the origin at the time t_1 there are now two conditions to satisfy rather than one, corresponding to the two axes of the polarization ellipse; see equation (8). This is one condition too many. In other words, the electron will, in general, not return if it is released with zero velocity. Classically, for rescattering the electron does not have to return exactly to the center of the potential. Quantum-mechanically, the ISFA as described above remains perfectly applicable: the solutions of the saddle-point equations (16) will automatically do the job. One just has to find them, which may not be straightforward.

To see this more clearly, we first note that for elliptical rather than linear polarization the saddle-point equations (16) no longer have real solutions when $I_p = 0$ (unless the momentum **p** has special values to be discussed below). This follows from equation (16b): if both components of the initial velocity are zero, then, if the electron returns in one direction, it cannot return in the other. However, it is clear that with a suitable *nonzero* initial momentum the electron will always be able exactly to return to its starting position. This initial velocity is automatically provided by the solution of the saddle-point equations (16). However, the larger it is, the larger are the imaginary parts, which suppress the corresponding partial ionization rate. Equation (16b) has the consequence that this momentum can be smaller if the travel time is large so that long orbits become more important compared with linear polarization.

The consequences can be inspected in figure 10, which shows an experimental electron spectrum at an angle of 30° to the direction of the major component of the polarization ellipse along with its quantum-orbit interpretation [104]. The spectrum exhibits two plateaus (between 10 and 25 eV and between 35 and 50 eV), which can be traced to different quantum orbits as depicted in the figure. The plateau that is highest in energy is generated by the shortest quantum orbits, but its yield is low. Namely, in order to return, these orbits require a large initial transverse momentum and, consequently, their contributions are suppressed. The plateau that is lower in energy is generated by longer orbits, which have a lower cutoff energy (see above) and a higher yield. The theory predicts a third plateau in between the former two, which, however, is hardly visible in the data. More theoretical details for HATI by an elliptically polarized laser field can be
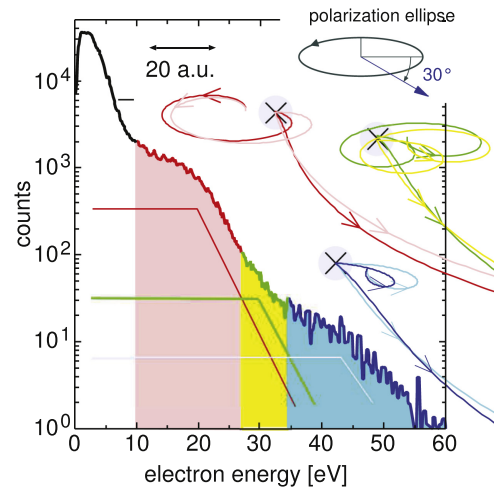

Figure 10. ATI spectrum in xenon recorded at the angle of 30° to the major axis of the polarization ellipse of an elliptically polarized laser field ($\xi = 0.36$), as depicted in the upper right corner. The wavelength is 800 nm and the intensity 7.7×10^{13} W cm^{-2}. Two different plateaus can be recognized, which are shaded in different colors, along with the quantum orbits that are responsible for them. The position of the atom is indicated by a cross mark. Note that the orbits start at the exit of the tunnel, not at the position of the atom. (A third plateau in between the former two is predicted by theory but hardly visible in the data.) From [104]. Reprinted with permission from AAAS.

found in [10, 141]. Another more recent experiment that supports this quantum-orbit interpretation is reported in [142].

We should mention that for elliptical polarization and *special values of* **p**, there are real solutions of the saddle-point equations for $I_p = 0$, namely those where $\mathbf{p} + \mathbf{A}(t) = \mathbf{0}$ for some time t. Actually, these are the most important solutions. For example, they imply that the maximum of the ATI spectrum for a long circularly polarized pulse occurs at $E = U_p$. For a circularly polarized few-cycle pulse, the solutions of the condition $\mathbf{p} + \mathbf{A}(t) = \mathbf{0}$ (whether there is one or more than one) predict whether and in which direction the ATI spectrum will display interference fringes [143].

4. Absolute phase measurement—an application of the ATI plateau

For several years following its discovery in 1993, the ATI plateau had been considered to be of academic interest only in stark contrast to the related effect of HHG. Today, the ATI plateau has become the backbone of a powerful method for the measurement of the absolute phase, also known as the carrier-envelope (CE) phase. The underlying conjecture is that the spatial asymmetry of the electric field of few-cycle pulses will entail asymmetries in the photoelectron angular distributions. More precisely, the Curie symmetry principle [144, 145] implies that photoelectron angular distributions with no inversion symmetry must be caused by laser pulses that also lack inversion symmetry, which is only possible for few-cycle (or multi-color) laser pulses. In the following, we

will more descriptively speak of left-right asymmetries instead of broken inversion symmetry.

At first glance, using plateau photoelectrons rather than low-energy direct electrons seems counterproductive due to their comparatively small number. Indeed, researchers did initially consider low-energy electrons for phase measurement. However, this did not turn out to be very successful. In the perturbative regime, one would argue that continuum states of opposite parity but comparable amplitude must be superimposed in order to observe left-right asymmetries. Obviously, this can only happen in between adjacent ATI peaks—where the yield is low [146]. Nevertheless, the concept can be applied for, e.g., coherent control by few-cycle pulses [147]. In the strong-field regime, the situation is hardly more favorable: the high nonlinearity of tunnel ionization can certainly lead to strongly different ionization yield within subsequent optical half-cycles with opposite field direction. However, this asymmetry largely cancels out due to the fact that the photoelectrons will fly in direction of the vector potential $\mathbf{A}(t_0)$ at the instant of ionization t_0, as discussed above (see figure 2 in [148]). The situation is more advantageous for circular polarization [149] where the vector potential does not change sign in the middle of each half-cycle. Therefore, circular polarization was used in the first detection of absolute phase effects [143, 150].

The phase dependence of plateau electrons, i.e. rescattered electrons, is much stronger. Qualitatively, this is not hard to see: in order to obtain a high yield of high-energy photoelectrons, the field strength within the laser pulse needs to be as high as possible (i) at the instant t_0 of ionization—otherwise the tunneling probability will be low and no photoelectrons are created—and (ii) in the optical cycle following the instant t_1 of recollision—otherwise the photoelectron cannot be accelerated to high energies. For few-cycle pulses, these requirements are necessarily in conflict because t_0 and t_1 are separated by almost one optical cycle. Tuning the absolute phase φ can be used to find the best compromise, which will be the worst compromise in the opposite emission direction.

Experimentally, a so-called stereo time-of-flight (stereo-TOF) photoelectron spectrometer consisting of two opposing TOF spectrometers is used (see figure 11). The laser polarization is parallel to the spectrometer axis. The expectations with regard to phase sensitivity of direct and rescattered electrons are completely fulfilled. In order to quantify the effects, the asymmetry A has been introduced. It is the difference of the numbers N of photoelectrons emitted in opposite directions ('left' and 'right') normalized to their sum: $A := (N_{\text{left}} - N_{\text{right}})/(N_{\text{left}} + N_{\text{right}})$. Alternatively, the ratio can be used. For direct electrons, A is on the order of 10%, while it approaches 100% for plateau electrons [151]. Other phenomena that can be observed in such experiments are a dependence on the Gouy phase [152, 153] and a phase dependence of the ATI peak contrast [154], which has an appealing interpretation as a double-slit experiment in time [155]. The stereo-ATI phase meter can also be utilized to reconstruct a few-cycle laser pulse with arbitrary polarization [156].

In order to turn the experiment into a measurement device capable of measuring the absolute phase of each and every laser pulse at multi-kHz pulse repetition rates [159], an instrument optimized for photoelectron production and collection efficiency as well as sophisticated but fast data acquisition hard- and software were developed. An important insight has been that the phase dependence of the asymmetry depends on the electron energy. In fact, two energy intervals 'low' and 'high' can be found within the ATI plateau such that the phase dependence of A_{low} and A_{high} differ by 90°. Then, if A_{high} is plotted versus A_{low} for each laser pulse, this parametric plot will be of an approximately circular shape. The azimuthal angle for each data point represents an individual laser pulse. It corresponds to the absolute phase of this laser pulse modulo a certain offset that can be determined by comparison with experiments and simulations with atomic hydrogen [160]. A particularly useful side effect is the dependence of the asymmetry, or, equivalently, the radius of the parametric asymmetry plot, on the pulse duration: the longer the pulse is, the smaller are the asymmetry and the radius. This can be exploited to measure the duration of few-cycle pulses [161]. In contrast to conventional laser pulse metrology, this approach becomes more sensitive for shorter pulses. In addition, the method is robust and fast. For a review, see [162].

Single-shot phase measurement with inherent laser performance monitoring has enabled a new class of experiments on the phase dependence of the interaction of few-cycle pulses with matter: phase stabilization is put aside. Rather the phase of each pulse is measured and the data obtained concurrently are 'tagged' with this phase [163]. Later, the data can be sorted and the phase dependence of the effect under investigation can be reconstructed. Phase-tagging has enabled a number of experiments with low event rate and correspondingly large data acquisition times, see, e.g., [153, 164–167].

5. A classical view of the LES

All theoretical simulations reported so far were based on the quantum-mechanical SFA or ISFA, which implies that after its liberation the electron experiences the Coulomb potential either not at all or at most once (in the sense of quantum-mechanical perturbation theory). For a completely different point of view, we will turn to a description where the liberated electron is treated entirely classically, by solving Newton's equation of motion. Hence, both fields—the laser field and the Coulomb field—are on the same footing all of the time. Models of this type have been frequently applied, mostly in the context of nonsequential double ionization where the trajectories of two electrons have to be followed; for a review, see, e.g. [168]. The first electron may be injected into the continuum according to a quantum-mechanical tunneling formula [169] or the process in its entirety is treated classically starting from a microcanonical ensemble [170]. The description to be outlined below differs from most others by
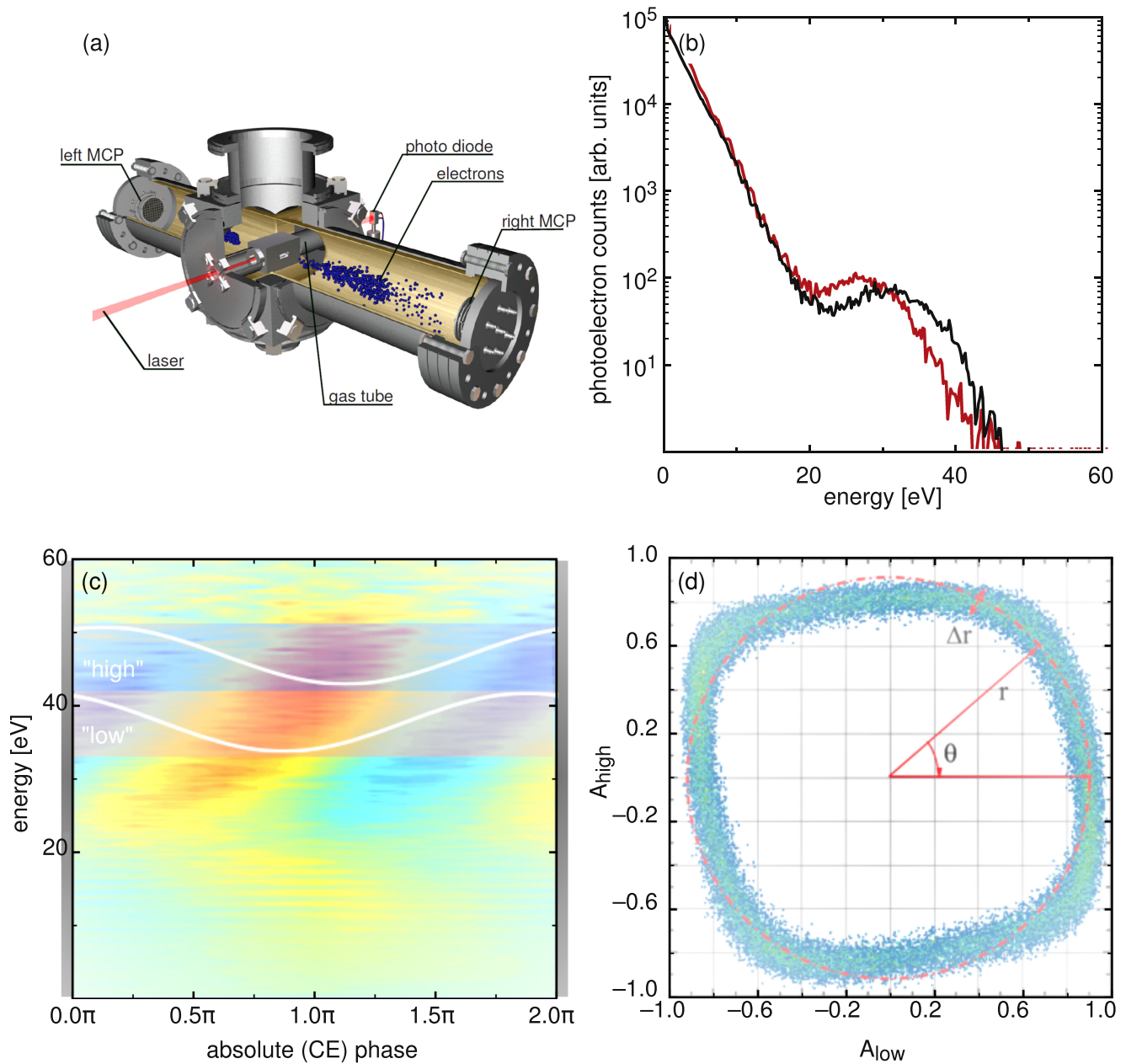
Figure 11. (a) Stereo-ATI phase meter: few-cycle laser pulses of horizontal polarization ionize xenon atoms inside a vacuum apparatus. The photoelectrons emitted to the left and the right are detected time-resolved with microchannel plate (MCP) detectors. (b) For any given absolute phase (here $\varphi = 0$), the spectra detected on the left (red) and right (black) detector differ in a characteristic way, but always more for rescattered ($E > 20$ eV) than for direct ($E < 20$ eV) electrons. ISFA calculations of such phase-dependent spectra can be found in [157, 158]. (c) Asymmetry $A(\varphi, E)$ as a function of absolute phase and photoelectron energy. From spectra as displayed in (b), the asymmetry $A := (N_{left} - N_{right})/(N_{left} + N_{right})$ is computed for all phases and plotted in false colors. Red (blue) shades indicate that more electrons are emitted to the left (right). The white sine-like curves indicate the evolution of the asymmetry in the low- and high-energy part of the ATI plateau. The low- and high-energy interval can be chosen such that $A(E_{low})$ and $A(E_{high})$ have a phase difference of 90°. (d) Therefore, if $A(E_{low})$ and $A(E_{high})$ are determined for each laser pulse and used as coordinates, a more or less circular plot is produced. The azimuthal angle θ is identical to the absolute phase φ, apart from a constant offset angle. The radius r of the asymmetry plot can be used to determine the pulse duration.

taking advantage of the fact that for linear polarization the motion of the liberated electron unfolds in a plane.

We proceed by starting classical trajectories at the exit of the tunnel [171–173]. At the time t_0 when the electron becomes free, we fix its initial velocity, viz. the transverse component $v_y(t_0) = v_0$ and the longitudinal component, which we set to zero, $v_x(t_0) = 0$. As just mentioned, we take

advantage of the fact that the classical motion is confined to the plane defined by the electric field and the initial transverse velocity, and we follow the electron kinematics in this plane. That is, we consider the mapping, mediated by the equations of motion, of initial conditions (t_0, v_0) onto the plane of final momenta (p_x, p_y) at the end of the laser pulse. Without the Coulomb field, $v_y(t)$ is conserved, and the final longitudinal
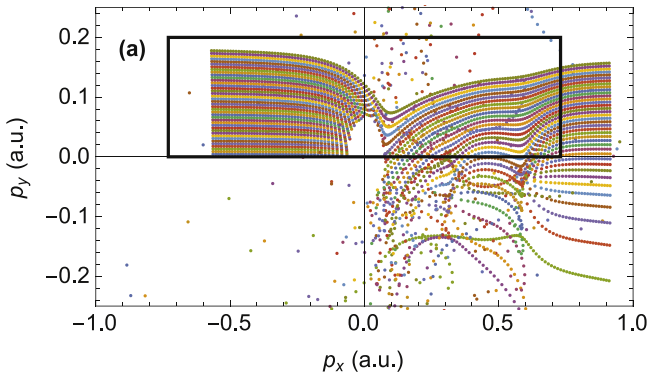
J. Phys. B: At. Mol. Opt. Phys. **51** (2018) 162002

Topical Review

Figure 12. Mapping of the horizontal lines $75° < \omega t_0 < 105°$, $0.005 < v_0 < 0.2$ a.u. of initial conditions on the final-momentum plane (p_x, p_y) at the end of a long laser pulse (36 cycles). The parameters are those of the experiment [56]: argon ($I_p = 0.579$ a.u.), $U_p = 56.1$ eV, $\lambda = 2 \, \mu$m. The corresponding LES momentum from equation (9) is $p_x = 0.61$ a.u. ($E = 5.05$ eV). Without the Coulomb field, the initial data would be mapped into the inside of the rectangle in the upper half plane. With the Coulomb field, the results of the mapping by the equations of motion are represented by the colored dots.

momentum outside the laser field will be $-A(t_0)$ (we consider linear polarization). In this way, a horizontal line (t_0, v_0) of initial conditions, where t_0 is from some interval and $v_0 = $ const, is mapped on a horizontal line in the plane of final momenta, filling the inside of a rectangle as shown in figure 12 [172]. With the Coulomb field, horizontal lines are no longer mapped on horizontal lines. Therefore, figure 12 very clearly visualizes the effects of the Coulomb field.

We see that the larger the initial transverse momentum v_0 is and the earlier (before a peak of the field) the electron starts, the smaller is the effect of the Coulomb potential. On the other hand, electrons that start close to a peak (close to $\omega t_0 = 90°$) with small transverse momentum are completely thrown off course by the Coulomb field. The dots scattered over the plot reflect the fact that in a part of this region the mapping is chaotic, in the sense of a sensitive dependence on the initial conditions (see, e.g., [174]). Other electrons from this region end up with negative energy at the end of the pulse, i.e., they remain bound [171, 175]. The respective points were eliminated from figure 12 giving rise to the empty area around zero momentum. For trajectories with positive final energy, the most eye-catching effect is that their transverse velocity may even change its sign so that the fourth quadrant becomes populated. It is these electrons that form the LES discussed above (this was first observed in [67]). A structure below $p_x = 0.59$ a.u. is clearly visible, which corresponds to $p_{LES,1} = 0.61$ a.u. from equation (9). The next LES at $p_{LES,2} = 0.37$ a.u. is also noticeable. With better statistics, it becomes visible that the LES corresponds to a caustic of the afore-mentioned mapping and its structure can be classified in terms of catastrophe theory [173].

Conceptually, the two approaches—the simple-man picture and the quantum-mechanical ISFA versus the classical equations of motion—could hardly be more different. In the ISFA, in first-order Born approximation according to

equation (15), the wave packet of the liberated electron interacts with the ion just once while the laser field is taken care of exactly. Solving, on the other hand, the classical equation of motion both fields are treated exactly and on the same footing. Nonetheless, the phenomenology of the effects produced is the same, and the agreement is even semi-quantitative. Part of an explanation can be found in the fact that for pure Coulomb scattering the quantum-mechanical lowest-order Born approximation happens to yield the exact scattering cross section, which, moreover, agrees with the classical result. But, of course, Coulomb scattering on the background of a laser field is a vastly more complex problem.

6. Conclusions

We have given a highly personal review of the history of the above-threshold-ionization plateau and its various features. The allure of the plateau and of intense-laser-atom physics in general is their basic simplicity. Yet subtle and not so subtle quantum-mechanical effects are never far below the surface. No longer an effect of academic interest only, the plateau and its properties are employed by current methods to determine the laser intensity and the absolute phase and duration of a few-cycle pulse. The plateau has also provided novel tools to extract scattering potentials from atomic and molecular data and may lend itself to further insightful analysis in the future.

ORCID iDs

W Becker ⓘ https://orcid.org/0000-0001-8939-0372
D B Milošević ⓘ https://orcid.org/0000-0001-5060-3318

References

[1] L'Huillier A, Lompré L, Mainfray G and Manus C 1982 *Phys. Rev. Lett.* **48** 1814
[2] L'Huillier A, Lompré L, Mainfray G and Manus C 1983 *J. Phys. B: At. Mol. Phys.* **16** 1363
[3] McPherson A, Gibson G, Jara H, Johann U, Luk T S, McIntyre I A, Boyer K and Rhodes C K 1987 *J. Opt. Soc. Am.* B **4** 595
[4] Ferray M, L'Huillier A, Li X F, Lompré L, Mainfray G and Manus C 1988 *J. Phys. B: At. Mol. Opt. Phys.* **21** L31
[5] Li X F, L'Huillier A, Ferray M, Lompré L and Mainfray G 1989 *Phys. Rev.* A **39** 5751
[6] Paulus G G, Nicklich W, Xu H, Lambropoulos P and Walther H 1994 *Phys. Rev. Lett.* **72** 2851
[7] Lewenstein M, Ivanov M, Balcou P, L'Huillier A and Corkum P B 1994 *Phys. Rev.* A **49** 2117

J. Phys. B: At. Mol. Opt. Phys. **51** (2018) 162002

Topical Review

[8] Lewenstein M, Kulander K C, Bucksbaum P H and Schafer K J 1995 *Phys. Rev.* A **51** 1495

[9] Kopold R, Becker W and Kleber M 2000 *Opt. Commun.* **179** 39

[10] Kopold R, Milošević D B and Becker W 2000 *Phys. Rev. Lett.* **84** 3831

[11] Kling M F and Vrakking M J J 2008 *Annu. Rev. Phys. Chem.* **59** 463

[12] Krausz F and Ivanov M 2009 *Rev. Mod. Phys.* **81** 163

[13] Nisoli M and Sansone G 2009 *Prog. Quantum Electron.* **33** 17

[14] Ueda K and Ishikawa K L 2011 *Nat. Phys.* **7** 371

[15] Corkum P B 1993 *Phys. Rev. Lett.* **71** 1994

[16] Kulander K C, Schafer K J and Krause K 1993 *Super-Intense Laser-Atom Physics* ed B Piraux *et al* (New York: Plenum Press) p 95

[17] Fittinghoff D, Bolton P, Chang B and Kulander K C 1992 *Phys. Rev. Lett.* **69** 2642

[18] Budil K S, Salières P, L'Huillier A, Ditmire T and Perry M D 1993 *Phys. Rev.* A **48** R3437

[19] Ivanov M, Dietrich P, Burnett N H and Corkum P B 1994 *Phys. Rev.* A **50** R3585

[20] Weber T, Dörner R, Giessen H, Weckenbrock M, Urbasch G, Staudte A, Spielberger L, Jagutzki O, Mergel V and Vollmer M 2000 *Nature* **405** 658

[21] Moshammer R *et al* 2000 *Phys. Rev. Lett.* **84** 447

[22] Yang B, Schafer K J, Walker B, Kulander K C, Agostini P and DiMauro L 1993 *Phys. Rev. Lett.* **71** 3770

[23] Paulus G G, Becker W, Nicklich W and Walther H 1994 *J. Phys. B: At. Mol. Opt. Phys.* **27** L703

[24] Niikura H, Légaré F, Hasbani R, Bandrauk A D, Ivanov M Y, Villeneuve D M and Corkum P B 2002 *Nature* **417** 917

[25] Spanner M, Smirnova O, Corkum P B and Ivanov M Y 2004 *J. Phys. B.: At. Mol. Opt. Phys.* **37** L243

[26] Meckel M *et al* 2008 *Science* **320** 1478

[27] Okunishi M, Morishita T, Prümper G, Shimada K, Lin C D, Watanabe S and Ueda K 2008 *Phys. Rev. Lett.* **100** 143001

[28] Ray D *et al* 2008 *Phys. Rev. Lett.* **100** 143002

[29] Čerkić A, Hasović E, Milošević D B and Becker W 2009 *Phys. Rev.* A **79** 033413

[30] Frolov M V, Manakov N L and Starace A F 2009 *Phys. Rev.* A **79** 033406

[31] Milošević D B, Becker W, Okunishi M, Prümper G, Shimada K and Ueda K 2010 *J. Phys. B: At. Mol. Opt. Phys.* **43** 015401

[32] Gazibegović-Busuladžić A *et al* 2011 *Phys. Rev.* A **84** 043426

[33] Muller H G and van Linden van den Heuvell B 1988 *Multiphoton Processes: Proceedings of ICOMP 4* ed S J Smith and P L Knight (Cambridge: Cambridge University Press) pp 25–34

[34] Becker W, Grasbon F, Kopold R, Milošević D B, Paulus G G and Walther H 2002 *Advances in Atomic, Molecular, and Optical Physics* vol 48 (New York: Academic) 35–98

[35] Milošević D B and Ehlotzky F 2003 *Advances in Atomic, Molecular, and Optical Physics* vol 49 (Amsterdam: Elsevier) pp 373–532

[36] Becker A and Faisal F H M 2005 *J. Phys. B: At. Mol. Opt. Phys.* **38** R1

[37] Milošević D B, Paulus G G, Bauer D and Becker W 2006 *J. Phys. B: At. Mol. Opt. Phys.* **39** R203

[38] Lin C D, Le A-T, Chen Z, Morishita T and Lucchese R 2010 *J. Phys. B: At. Mol. Opt. Phys.* **43** 122001

[39] Agostini P and DiMauro L F 2012 *Advances in Atomic, Molecular, and Optical Physics* vol 61 (Amsterdam: Elsevier) pp 117–158

[40] Popruzhenko S V 2014 *J. Phys. B: At. Mol. Opt. Phys.* **47** 204001

[41] Le A-T, Wei H, Jing C and Lin C D 2016 *J. Phys. B: At. Mol. Opt. Phys.* **49** 053001

[42] Gallagher T F 1988 *Phys. Rev. Lett.* **61** 2304

[43] Maharjan C M, Ghimire S, Alnaser A S, Tong X M, Ulrich B, Ranitovic P, Chang Z, Litvinyuk I V and Cocke C 2005 *Phys. Rev.* A **72** 041403

[44] Eckle P, Smolarski M, Schlup P, Biegert J, Staudte A, Schöffler M, Muller H G, Dörner R and Keller U 2008 *Nat. Phys.* **4** 565

[45] Eckle P, Muller H G, Pfeiffer A N, Cirelli C, Staudte A, Dörner R, Büttiker M and Keller U 2008 *Science* **322** 1525

[46] Pfeiffer A N, Cirelli C, Smolarski M, Dimitrovski D, Abu-samha M, Madsen L B and Keller U 2012 *Nat. Phys.* **8** 76

[47] Wustelt P, Möller M, Rathje T, Sayler A M, Stöhlker T and Paulus G G 2015 *Phys. Rev.* A **91** 031401

[48] Paulus G G, Zacher F, Walther H, Lohr A, Becker W and Kleber M 1998 *Phys. Rev. Lett.* **80** 484

[49] Landsman A S and Keller U 2015 *Phys. Rep.* **547** 1

[50] Pazourek R, Nagele S and Burgdörfer J 2015 *Rev. Mod. Phys.* **87** 765

[51] Goreslavski S P, Paulus G G, Popruzhenko S V and Shvetsov-Shilovski N I 2004 *Phys. Rev. Lett.* **93** 233002

[52] Popruzhenko S V, Paulus G G and Bauer D 2008 *Phys. Rev.* A **77** 053409

[53] Torlina L *et al* 2015 *Nat. Phys.* **11** 503

[54] Paulus G G, Becker W and Walther H 1995 *Phys. Rev.* A **52** 4043

[55] Möller M, Meyer F, Sayler A M, Paulus G G, Kling M F, Schmidt B E, Becker W and Milošević D B 2014 *Phys. Rev.* A **90** 023412

[56] Blaga C I, Catoire F, Colosimo P, Paulus G G, Muller H G, Agostini P and DiMauro L 2009 *Nat. Phys.* **5** 335

[57] Quan W *et al* 2009 *Phys. Rev. Lett.* **103** 093001

[58] Colosimo P 2007 A study of wavelength dependence of strong-field optical ionization *PhD Thesis* Stony Brook University

[59] Faisal F H M 2009 *Nat. Phys.* **5** 319

[60] Becker W, Goreslavski S P, Milošević D B and Paulus G G 2014 *J. Phys. B: At. Mol. Opt. Phys.* **47** 204022

[61] Kästner A, Saalmann U and Rost J M 2012 *Phys. Rev. Lett.* **108** 033201

[62] Kästner A, Saalmann U and Rost J M 2012 *J. Phys. B: At. Mol. Opt. Phys.* **45** 074011

[63] Milošević D B 2014 *Phys. Rev.* A **90** 063414

[64] Milošević D B 2016 *J. Phys. B: At. Mol. Opt. Phys.* **49** 175601

[65] Guo L *et al* 2013 *Phys. Rev. Lett.* **110** 013001

[66] Liu C and Hatsagortsyan K Z 2010 *Phys. Rev. Lett.* **105** 113003

[67] Yan T-M, Popruzhenko S V, Vrakking M J J and Bauer D 2010 *Phys. Rev. Lett.* **105** 253002

[68] Lemell C, Dimitriou K I, Tong X-M, Nagele S, Kartashov D V, Burgdörfer J and Gräfe S 2012 *Phys. Rev.* A **85** 011403

[69] Lemell C, Burgdörfer J, Gräfe S, Dimitriou K I, Arbó D G and Tong X-M 2013 *Phys. Rev.* A **87** 013421

[70] Zhang K *et al* 2016 *Phys. Rev.* A **93** 021403

[71] Wu C Y, Yang Y D, Liu Y Q, Gong Q H, Wu M, Liu X, Hao X L, Li W D, He X T and Chen J 2012 *Phys. Rev. Lett.* **109** 043001

[72] Dura J *et al* 2013 *Sci. Rep.* **3** 2675

[73] Diesen E, Saalmann U, Richter M, Kunitski M, Dörner R and Rost J M 2016 *Phys. Rev. Lett.* **116** 143006

[74] Becker W and Milošević D B 2015 *J. Phys. B: At. Mol. Opt. Phys.* **48** 151001

[75] Wolter B *et al* 2014 *Phys. Rev.* A **90** 063424

[76] Wolter B, Pullen M G, Baudisch M, Sclafani M, Hemmer M, Senftleben A, Schröter C D, Ullrich J, Moshammer R and Biegert J 2015 *Phys. Rev.* X **5** 021034

[77] Moshammer R *et al* 2003 *Phys. Rev. Lett.* **91** 113002

[78] Dimitriou K I, Arbó D G, Yoshida S, Persson E and Burgdörfer J 2004 *Phys. Rev.* A **70** 061401(R)

[79] Kopold R 2001 Atomare ionisationsdynamik in starken laserfeldern *PhD Thesis* Technische Universität München

[80] Hasović E, Busuladžić M, Gazibegović-Busuladžić A, Milošević D B and Becker W 2007 *Laser Phys.* **17** 376

[81] Milošević D B, Hasović E, Busuladžić M, Gazibegović-Busuladžić A and Becker W 2007 *Phys. Rev.* A **76** 053410

[82] Milošević D B, Bauer D and Becker W 2006 *J. Mod. Opt.* **63** 125

[83] Bauer D, Milošević D B and Becker W 2006 *J. Mod. Opt.* **63** 135

[84] Gaarde M B, Schafer K J, Kulander K C, Sheehy B, Kim D and DiMauro L 2000 *Phys. Rev. Lett.* **84** 2822

[85] Chen Z, Le A-T, Morishita T and Lin C D 2009 *Phys. Rev.* A **79** 033409

[86] Keldysh L 1965 *Sov. Phys.—JETP* **20** 1307

[87] Perelomov A M, Popov V S and Terent'ev M V 1966 *Sov. Phys.—JETP* **23** 924

[88] Faisal F H M 1973 *J. Phys. B: At. Mol. Phys.* **6** L89

[89] Reiss H R 1980 *Phys. Rev.* A **22** 1786

[90] Becker W, Lohr A and Kleber M 1994 *J. Phys. B: At. Mol. Opt. Phys.* **27** L325

[91] Becker W, Lohr A and Kleber M 1995 *J. Phys. B: At. Mol. Opt. Phys.* **28** 1931

[92] Bao D, Chen S-G and Liu J 1996 *Appl. Phys.* B **62** 313

[93] Lohr A, Kleber M, Kopold R and Becker W 1997 *Phys. Rev.* A **55** R4003

[94] Milošević D B and Ehlotzky F 1998 *Phys. Rev.* A **57** 5002

[95] Milošević D B and Ehlotzky F 1998 *Phys. Rev.* A **58** 3124

[96] Smirnov M B and Krainov V P 1998 *J. Phys. B: At. Mol. Opt. Phys.* **31** L519

[97] Goreslavski S P and Popruzhenko S V 1998 *Phys. Lett.* A **249** 477

[98] Goreslavskii S P and Popruzhenko S V 1999 *J. Phys. B: At. Mol. Opt. Phys.* **32** L531

[99] Schyja V, Lang T and Helm H 1998 *Phys. Rev.* A **57** 3692

[100] Korneev P A *et al* 2012 *Phys. Rev. Lett.* **108** 223601

[101] Korneev P A, Popruzhenko S V, Goreslavski S P, Becker W, Paulus G G, Fetić B and Milošević D B 2012 *New J. Phys.* **14** 055019

[102] Huismans Y *et al* 2011 *Science* **331** 61

[103] Bian X-B, Huismans Y, Smirnova O, Yuan K-J, Vrakking M J J and Bandrauk A D 2011 *Phys. Rev.* A **84** 043420

[104] Salières P *et al* 2001 *Science* **292** 902

[105] Milošević D B 2013 *J. Math. Phys.* **54** 042101

[106] Milošević D B 2017 *Phys. Rev.* A **96** 023413

[107] Yan T-M and Bauer D 2012 *Phys. Rev.* A **86** 053403

[108] Torlina L and Smirnova O 2012 *Phys. Rev.* A **86** 043408

[109] Kaushal J and Smirnova O 2013 *Phys. Rev.* A **88** 013421

[110] Li M, Geng J-W, Han M, Liu M-M, Peng L-Y, Gong Q and Liu Y 2016 *Phys. Rev.* A **93** 013402

[111] Lai X-Y, Poli C, Schomerus H and Figueira de Morisson Faria C 2015 *Phys. Rev.* A **92** 043407

[112] Shvetsov-Shilovski N I, Lein M, Madsen L B, Räsänen E, Lemell C, Burgdörfer J, Arbó D G and Tőkési K 2016 *Phys. Rev.* A **94** 013415

[113] Keil T, Popruzhenko S V and Bauer D 2016 *Phys. Rev. Lett.* **117** 243003

[114] Lai X, Yu S, Huang Y, Hua L, Gong C, Quan W, Figueira de Morisson Faria C and Liu X 2017 *Phys. Rev.* A **96** 013414

[115] Shvetsov-Shilovski N I and Lein M 2018 *Phys. Rev.* A **97** 013411

[116] Maxwell A S, Al-Jawahiry A, Lai X Y and Figueira de Morisson Faria C 2018 *J. Phys. B: At. Mol. Opt. Phys.* **51** 124001

[117] Gribakin G F and Kuchiev M Y 1997 *Phys. Rev.* A **55** 3760

[118] Kiyan I Y and Helm H 2003 *Phys. Rev. Lett.* **90** 183001

[119] Milošević D B, Gazibegović-Busuladžić A and Becker W 2003 *Phys. Rev.* A **68** 050702(R)

[120] Frolov M V, Manakov N L, Pronin E A and Starace A F 2003 *Phys. Rev. Lett.* **91** 053003

[121] Gazibegović-Busuladžić A, Milošević D B, Becker W, Bergues B, Hultgren H and Kiyan I Y 2010 *Phys. Rev. Lett.* **104** 103004

[122] Popruzhenko S V, Korneev P A, Goreslavski S P and Becker W 2002 *Phys. Rev. Lett.* **89** 2117

[123] Bucksbaum P H, Muller H G and Hertlein M 1997 *J. Phys. B: At. Mol. Opt. Phys.* **30** L197

[124] Hansch P, Walker M and Van Woerkom L 1997 *Phys. Rev.* A **55** R2535

[125] Muller H G 1999 *Phys. Rev. Lett.* **83** 3158

[126] Muller H G 1999 *Phys. Rev.* A **60** 1341

[127] Nandor M J, Walker M A and Van Woerkom L 1998 *J. Phys. B: At. Mol. Opt. Phys.* **31** 4617

[128] Nandor M, Walker M, Van Woerkom L and Muller H G 1999 *Phys. Rev.* A **60** R1771

[129] Paulus G G, Grasbon F, Walther H, Kopold R and Becker W 2001 *Phys. Rev.* A **64** 021401(R)

[130] Muller H G 2001 *Opt. Exp.* **8** 44

[131] Muller H G 2001 *Opt. Exp.* **8** 86

[132] Wassaf J, Taïeb R, Véniard V and Maquet A 2003 *Phys. Rev. Lett.* **90** 013003

[133] Potvliege R M and Vučić S 2006 *Phys. Rev.* A **74** 023412

[134] Borca B, Frolov M, Manakov N and Starace A F 2002 *Phys. Rev. Lett.* **88** 193001

[135] Frolov M V, Khukivadze A A, Manakov N L and Starace A F 2006 *J. Phys. B: At. Mol. Opt. Phys.* **39** S283

[136] Krajewska K, Fabrikant I I and Starace A F 2007 *Laser Phys.* **17** 368

[137] Wigner E P 1948 *Phys. Rev.* **73** 1002

[138] Baz A I 1958 *Sov. Phys.—JETP* **6** 709

[139] Grasbon F, Paulus G G, Walther H, Villoresi P, Sansone G, Stagira S, Nisoli M and De Silvestri S 2003 *Phys. Rev. Lett.* **91** 173003

[140] Milošević D B and Becker W 2002 *Phys. Rev.* A **66** 063417

[141] Paulus G G, Grasbon F, Dreischuh A, Walther H, Kopold R and Becker W 2000 *Phys. Rev. Lett.* **84** 3791

[142] Lai X, Wang C, Chen Y, Hu Z, Quan W, Liu X, Chen J, Cheng Y, Xu Z and Becker W 2013 *Phys. Rev. Lett.* **110** 043002

[143] Milošević D B, Paulus G G and Becker W 2002 *Phys. Rev. Lett.* **89** 153001

[144] Curie P 1894 *J. Phys. Theor. Appl.* **3** 393

[145] Chalmers A F 1970 *Br. J. Phil. Sci.* **21** 133

[146] Cormier E and Lambropoulos P 1998 *Eur. Phys. J.* D **2** 15

[147] Rathje T, Sayler A M, Zeng S, Wustelt P, Figger H, Esry B D and Paulus G G 2013 *Phys. Rev. Lett.* **111** 093002

[148] Paulus G G, Lindner F, Milošević D B and Becker W 2004 *Phys. Scr.* **110** 120

[149] Dietrich P, Krausz F and Corkum P B 2000 *Opt. Lett.* **25** 16

[150] Paulus G G, Grasbon F, Walther H, Villoresi P, Nisoli M, Stagira S, Priori E and De Silvestri S 2001 *Nature* **414** 182

[151] Paulus G G, Lindner F, Walther H, Baltuška A, Goulielmakis E, Lezius M and Krausz F 2003 *Phys. Rev. Lett.* **91** 253004

[152] Lindner F, Paulus G G, Walther H, Baltuška A, Goulielmakis E, Lezius M and Krausz F 2004 *Phys. Rev. Lett.* **92** 113001

J. Phys. B: At. Mol. Opt. Phys. **51** (2018) 162002

Topical Review

[153] Hoff D, Krüger M, Maisenbacher L, Sayler A M, Paulus G G and Hommelhoff P 2017 *Nat. Phys.* **110** 1251

[154] Lindner F, Schätzel M, Walther H, Baltuška A, Goulielmakis E, Krausz F, Milošević D B, Bauer D, Becker W and Paulus G G 2005 *Phys. Rev. Lett.* **95** 040401

[155] Rodgers P 2005 *Phys. World* **18** 5

[156] Popruzhenko S V, Shvetsov-Shilovski N I, Goreslavski S P, Becker W and Paulus G G 2007 *Opt. Lett.* **32** 1372

[157] Milošević D B, Paulus G G and Becker W 2003 *Opt. Exp.* **11** 1418

[158] Milošević D B, Paulus G G and Becker W 2004 *Laser Phys. Lett.* **1** 93

[159] Sayler A M, Rathje T, Müller W, Rühle K, Kienberger R and Paulus G G 2011 *Opt. Lett.* **36** 1

[160] Sayler A M *et al* 2015 *Opt. Lett.* **40** 3137

[161] Sayler A M, Rathje T, Müller W, Kürbis C, Rühle K, Stibenz G and Paulus G G 2011 *Opt. Exp.* **19** 4464

[162] Rathje T, Johnson N G, Möller M, Süßmann F, Adolph D, Kübel M, Kienberger R, Kling M F, Paulus G G and Sayler A M 2012 *J. Phys. B: At. Mol. Opt. Phys.* **45** 074003

[163] Johnson N G *et al* 2011 *Phys. Rev.* A **83** 013412

[164] Miura S *et al* 2014 *Chem. Phys. Lett.* **595** 61

[165] Xie X *et al* 2014 *Phys. Rev. Lett.* **112** 163003

[166] Kübel M, Dube Z, Naumov A Y, Spanner M, Paulus G G, Kling M F, Villeneuve D M, Corkum P B and Staudte A 2017 *Phys. Rev. Lett.* **119** 183201

[167] Carpeggiani P *et al* 2017 *Nat. Photon.* **11** 383

[168] Becker W, Liu X, Ho P J and Eberly J H 2012 *Rev. Mod. Phys.* **84** 1011

[169] Chen J and Nam C H 2002 *Phys. Rev.* A **66** 053415

[170] Panfili R, Haan S L and Eberly J H 2002 *Phys. Rev. Lett.* **89** 113001

[171] Shvetsov-Shilovski N I, Goreslavski S P, Popruzhenko S V and Becker W 2009 *Laser Phys.* **19** 1550

[172] Kelvich S A, Becker W and Goreslavski S P 2016 *Phys. Rev.* A **93** 033411

[173] Kelvich S A, Becker W and Goreslavski S P 2017 *Phys. Rev.* A **96** 023427

[174] Goldstein H, Poole J P and Safko J L 2002 *Classical Mechanics* 3rd edn (Reading, MA: Addison-Wesley)

[175] Nubbemeyer T, Gorling K, Saenz A, Eichmann U and Sandner W 2008 *Phys. Rev. Lett.* **101** 233001